Electrochimica Acta 304 (2019) 513–520

Contents lists available at ScienceDirect

Electrochimica Acta

journal homepage: www.elsevier.com/locate/electacta

On the physical definition of dynamic impedance: How to design an optimal strategy for data extraction

Alberto Battistel [a, **], Fabio La Mantia [b, *]

[a] Department of Molecular Sciences and Nanosystems, University Cà Foscari Venice, Via Torino, 155B, 30172, Mestre, Venezia, Italy
[b] Universität Bremen, Energiespeicher- und Energiewandlersysteme, Bibliothekstr. 1, 28359, Bremen, Germany

ARTICLE INFO

Article history:
Received 20 January 2019
Received in revised form
1 March 2019
Accepted 4 March 2019
Available online 6 March 2019

Keywords:
Dynamic impedance spectroscopy
Volterra series
Dynamic multi-frequency analysis
FFT-EIS
Quadrature filter
Window function

ABSTRACT

Dynamic electrochemical impedance spectroscopy (DEIS) has attracted the interest of researchers due to its capability of acquiring impedance spectra of non-stationary systems in a broad range of frequencies. Although developed in the 70's, a physical definition of dynamic impedance, and in general of dynamic transfer function, is not present in literature. In this manuscript the general concept of dynamic frequency response is given in correlation to the Volterra series expansion: this can be used to define the ideal dynamic impedance response of an electrochemical system. It is clarified that DEIS is the intermodulation of the *ac* signal with the *dc* signal. Starting from this, different strategies for the extraction of the dynamic impedance spectra are compared, which are based on different heuristic definitions of DEIS. There are two main methodologies, one based on the use of window functions and the other on quadrature filters. Limits and merits of the different methodologies are discussed in the frame of the data analysis and data handling and show that window functions suffers at recovering low-frequencies impedances while quadrature filters work best in experiments which have a periodic or quasi-periodic trend.

1. Introduction

The idea of dynamic impedance was developed in the 70's, as a natural extension of the classic stationary impedance spectroscopy, however bearing some distinct features in the methodology. Classic impedance spectroscopy was usually measured one frequency at a time with a FRA (frequency response analyzer) or with a lock-in amplifier. Because of the delay between the measurement of every single frequency point in the impedance spectrum, Kramer and Kronig transforms were used to make sure that the spectrum was consistent. In other words, only those spectra that showed a sufficient degree of stationarity were retained. Of course if one injects all the frequencies at once, through a broadband multi-sine signal, the stationarity issue becomes less stringent. This was the first step toward the realization of dynamic impedance spectroscopy. The enormous improvements in the speed of analog-to-digital converters allowed employing broadband multi-sine signals with large frequency range and recording large datasets with high temporal accuracy, which could be analyzed by *fast Fourier transform* (FFT). Once the constraint on the stationarity is removed, the impedance during a cyclic voltammetry can be measured as a broadband implementation of the AC-voltammetry.

Already in the 70's Bond and Smith generalized the idea of AC-voltammetry [1–4]. They added a multisine on top of a voltammetry and broke the data recording in pieces in order to analyze each fragment through FFT. This idea is still in use nowadays and the method is usually referred to as FFT-EIS.

With time it was understood that there were limits on the application of FFT-EIS, in particular on the lowest frequency accessible. Different strategies were taken in order to push the lower frequency limit to smaller values. The multisine design was improved [5,6] and the concept of short-time Fourier transform with the use of window functions was taken into consideration ([5,7–10]). A baseline correction was also developed, in order to improve the performance of the FFT-EIS ([11–15]) by decreasing the spectral leakage.

However, the root of the problem lays on the reciprocity between time and frequency: exactly as it happens in quantum mechanics, where it is not possible to know simultaneously the speed and the position of an electron with arbitrary precision, time (σ_t)

* Corresponding author.
** Corresponding author.
E-mail addresses: alberto.battistel@rub.de (A. Battistel), lamantia@uni-bremen.de (F. La Mantia).

https://doi.org/10.1016/j.electacta.2019.03.033

and frequency resolution (σ_f) are bound by the Gabor limit (a generalization of the uncertainty principle):

$$\sigma_t \cdot \sigma_f \geq \frac{1}{4 \cdot \pi} \tag{1}$$

This brings to the natural conclusion that in estimating the dynamic impedance there is a natural insuperable trade-off between time and frequency resolution. The different methods used to recover the dynamic impedance simply offer different strategies to approach the trade-off.

It was already shown that the dynamic impedance ($Z(\omega,t)$) could be defined heuristically through two definitions. The first one is based on the short-term Fourier transforms and the use of a window function w with bandwidth bw (correlated with its width) centered at the time t [7–10,16,17]:

$$Z(\omega,t) = \frac{FT\left[\Delta u(t') \cdot w(t'-t,bw)\right]}{FT\left[I(t') \cdot w(t'-t,bw)\right]} \tag{2}$$

As usual the potential and current signals are expressed by Δu and I and the standard stationary impedance arises when the width of the window function approaches the total length of the dataset. On the other hand it is possible to define the dynamic impedance based on a quadrature filter $\tilde{g}$ with bandwidth bw centered around the frequencies of interest ω [17,18]:

$$Z(\omega,t) = \frac{iFT\left[\Delta\tilde{u}(\omega') \cdot \tilde{g}(\omega'-\omega,bw)\right]}{iFT\left[\tilde{I}(\omega') \cdot \tilde{g}(\omega'-\omega,bw)\right]} \tag{3}$$

where $\Delta\tilde{u}$ and $\tilde{I}$ are the Fourier transforms of the potential and current and iFT is the inverse Fourier transform. In this case standard stationary impedance arises when the filter bandwidth tends toward zero [17]. This definition reflects our use of filters in the dynamic multi-frequency analysis. Eqs. (2) and (3) reduce to the same if the Fourier transform of the window function w is equal to the filter $\tilde{g}$ [17].

Both definitions are however heuristic, *i.e.* are based on experimental extrapolation of the concept of impedance. In this work a physical definition of dynamic transfer function will be given and it will be shown how closely the methods developed by Bond, Harrington, and us are capable of recovering it.

2. Theoretical background

2.1. Volterra series and impedance spectroscopy

The concept of impedance and impedance spectra is often related to the linearized stationary behavior of a system; this is in general accepted as universal truth, as the way the impedance spectra are often measured, *i.e.* application of consecutive sine waves at different frequencies, does not allow the investigation of time variant non-linear systems. However, this is only an instrumental limitation, which can be easily overcome by the use of multisine signals. Indeed, the concept of impedance is just the linearization of the response signal of a non-linear system, and can be expressed in a general way through the following approximation of the Volterra series [19]:

$$Y(\omega,t) = \tilde{y}_1(\omega) + \sum_{n=2} \int_{-\infty}^{+\infty} \frac{\tilde{y}_n(\omega,\ldots,\tau_n)}{(n-1)!} \cdot \prod_{i=2}^{n} \Delta u_{dc}(t-\tau_i) \cdot d\tau_i \tag{4}$$

This is demonstrated in details in Appendix A of the supporting information. In Eq. (4), Y is the admittance (the inverse of the impedance), $\tilde{y}_n$ represent the Fourier transform of Volterra kernel of order n with respect to the variable τ_1 (dummy temporal variable), Δu_{dc} the non-linearizable part of the voltage signal, ω the angular frequency. The classic concept of stationary frequency response is obtained from Eq. (4) when Δu_{dc} is a step function and the value of the frequency response is calculated for the time that tends to infinite. The dependence of the stationary frequency response on the voltage, often observed in electrochemical systems, is a consequence of the non-linearity of the system, which is translated in values of the Volterra kernels of order two and above different from zero. In this case, it is also possible to define a time-dependent frequency response, as from Eq. (4). So, Eq. (4) can be considered as the physical definition of dynamic frequency response, while it remains still open the question on how this can be measured with the highest accuracy (the heuristic definition).

Using Eq. (4), it is also possible to model the ideal dynamic impedance of a system. If the physico-chemical phenomena governing the system can be translated in a mathematical form, it is also possible to calculate, often numerically, the dynamic impedance of a system. We have already shown [20] that the dynamic frequency response of a system does not change in shape (frequency dependence) due to the time variation if the frequency under investigation is sufficiently high. In general, the ideal dynamic frequency response of the system can be calculated through the set of equations:

$$\begin{aligned} &\boldsymbol{\tau}_{dc} \cdot \frac{\partial}{\partial t}\left(\frac{\tilde{\mathbf{x}}_{ac}(\omega,t)}{\Delta\tilde{u}_{ac}(\omega)}\right) + \left(i\cdot\omega\cdot\boldsymbol{\tau}_{dc} + \left.\frac{\partial\boldsymbol{\tau}}{\partial\mathbf{x}}\right|_{dc}\cdot\dot{\mathbf{x}}_{dc} - \left.\frac{\partial\mathbf{F}}{\partial\mathbf{x}}\right|_{dc}\right)\cdot\frac{\tilde{\mathbf{x}}_{ac}(\omega,t)}{\Delta\tilde{u}_{ac}(\omega)} \\ &\quad = -\left(\left.\frac{\partial\boldsymbol{\tau}}{\partial\Delta u}\right|_{dc}\cdot\dot{\mathbf{x}}_{dc} - \left.\frac{\partial\mathbf{F}}{\partial\Delta u}\right|_{dc}\right) \end{aligned} \tag{5}$$

$$\begin{aligned} Y(\omega,t) = &\left(\left.\frac{\partial I}{\partial\mathbf{x}}\right|_{dc} + i\cdot\omega\cdot\left.\frac{\partial I}{\partial\dot{\mathbf{x}}}\right|_{dc}\right)\cdot\frac{\tilde{\mathbf{x}}_{ac}(\omega,t)}{\Delta\tilde{u}_{ac}(\omega)} + \left.\frac{\partial I}{\partial\dot{\mathbf{x}}}\right|_{dc}\cdot\frac{\partial}{\partial t}\frac{\tilde{\mathbf{x}}_{ac}(\omega,t)}{\Delta\tilde{u}_{ac}(\omega)} \\ &+ \left(\left.\frac{\partial I}{\partial\Delta u}\right|_{dc} + i\cdot\omega\cdot\left.\frac{\partial I}{\partial\Delta\dot{u}}\right|_{dc}\right) \end{aligned} \tag{6}$$

Here, i is the imaginary unit, $\boldsymbol{x}$ is the vector of variables describing the system (concentration of species, potential, and so on…), $\boldsymbol{\tau}$ is a generic matrix of the time constants, I is the function describing the current intensity, the symbol ~ refers to the Fourier transform, the symbol · refers to the time derivatives, the subscript dc and ac refer to the non-linearizable and linearizable component of the variables, respectively. The detailed derivation of Eqs. (5) and (6) are given in Appendix B and C of the supporting information. To notice that, the classic stationary impedance can be calculated from the solution to equations (see also reference [21], with a proper change of symbols):

$$\left(i\cdot\omega\cdot\boldsymbol{\tau}_{dc} - \left.\frac{\partial\mathbf{F}}{\partial\mathbf{x}}\right|_{dc}\right)\cdot\frac{\tilde{\mathbf{x}}_{ac}(\omega)}{\Delta\tilde{u}_{ac}(\omega)} = \left.\frac{\partial\mathbf{F}}{\partial\Delta u}\right|_{dc} \tag{7}$$

$$Y(\omega) = \left(\left.\frac{\partial I}{\partial\mathbf{x}}\right|_{dc} + i\cdot\omega\cdot\left.\frac{\partial I}{\partial\dot{\mathbf{x}}}\right|_{dc}\right)\cdot\frac{\tilde{\mathbf{x}}_{ac}(\omega)}{\Delta\tilde{u}_{ac}(\omega)} + \left(\left.\frac{\partial I}{\partial\Delta u}\right|_{dc} + i\cdot\omega\cdot\left.\frac{\partial I}{\partial\Delta\dot{u}}\right|_{dc}\right) \tag{8}$$

Comparing Eq. (6) with Eq. (8) it is clear that an extra term containing the time derivatives of the Fourier transforms of all the variables is introduced. This together with the fact that $\boldsymbol{x}_{ac}$ depends on time produces the skirt of any multisine peak in the frequency domain.

For the aim of this work, it is important to stress that Eqs. (5) And (6) can be used to calculate the ideal dynamic frequency response of the system, which physical meaning is given in Eq. (4).

Now, the ideal dynamic frequency response of the system can be used to investigate the exactness of the heuristic definitions of dynamic frequency response, which have been introduced in literature (Eqs. (2) and (3)).

We want to stress that it is possible to observe the dynamic admittance in the dataset of the Fourier-transformed current. In fact, as shown in details in Appendix D of the supporting information, this appears as a skirt centered on the perturbed frequency and can be interpreted as the intermodulation of the *dc* signal with the *ac* signal [22–24] and represent the time-dependency of the system [25].

2.2. Different methods to extract Z(ω,t): FFT-EIS vs. DMFA

In literature, two main strategies are given for the recovery of the dynamic impedance spectra, *i.e.* FFT-EIS and dynamic multi-frequency analysis (DMFA), which differ only in the order in which the computational operations are performed. This is schematically represented in Fig. 1. Assuming a measurement of dynamic impedance, *Z(ω,t)*, was taken simultaneously to a cyclic voltammetry using a multisine, the dataset of the current would look like the first row of Fig. 1.

With the FFT-EIS method (left side) the dataset goes through three processes: *splitting, elaboration*, *Fourier transform (FT)*, and *dynamic impedance calculation (Z(ω,t) calculation)*.

In the *splitting,* the dataset is divided into smaller sections and each of these sections is elaborated singularly. Before the *FT*, the *elaboration* is necessary to reduce Gibbs phenomenon given by the discontinuity between the beginning and the end of the data section. The two main approaches are windowing [4,5,7–10,16], which brings both ends of the section smoothly to zero, and baseline correction [11,14], which reduces the DC difference. *De facto*, both approaches try to convert the data section into a ring, in the sense that the transition between the end and the beginning happens smoothly. Thereafter, FFT are applied on the elaborated section (*Fourier transform*) as if a *quasi-stationary* impedance was measured. A single value for each frequency of the multisine is taken for data section to calculate the impedance. This corresponds to take a single pseudo-stationary impedance spectrum which, in time, corresponds to the center of the section. Then the same process is repeated for the next section and the dynamic impedance corresponds to the sequence of impedance spectra calculated in every section (*dynamic impedance calculation*). The size of the sections and their overlapping is arbitrary and optimized according to the requirements. The time splitting can be seen as a recursive process, where the section to analyze slides through the dataset. The trend of the dynamic impedance is primarily influenced by the size of the split sections and therefore by the width of the window function with a trade-off between time and frequency resolution given by the size of the section.

For the dynamic multi-frequency analysis (DMFA, right side of Fig. 1), the four processes are performed in a different order. At first the whole dataset is transformed (*Fourier transform*), thereafter the frequency domain is split in sections around the frequencies of the multisine and around the zero frequency for the *dc* component (*splitting*). This step is followed by the use of the quadrature digital filter in each split section (*elaboration*). In the *dynamic impedance calculation*, every frequency section is then transformed back in the time domain and represents the trend of the dynamic impedance at that frequency. Gibbs phenomenon can be reduced working on the original dataset, by extension or mirroring. Mirroring process is described at the end of this article. The trend of the dynamic impedance for the DMFA is given by the shape of the digital filter and by its bandwidth.

2.3. Computational cost of FFT-EIS and DMFA

A first comparison between FFT-EIS and DMFA can be made on their computational costs and in both cases it can be considered that the highest cost comes from performing FFTs which cost is proportional to $L\cdot\log(L)$, L being the length of the data set to transform. For the FFT-EIS the cost is:

$$\mathrm{Cost}_{FFT-EIS} \propto n_Z \cdot l_w \cdot \log(l_w) \tag{9}$$

where n_Z is the number of dynamic impedance spectra to recover and l_w is the width of every single window. In general $n_Z \cdot l_w > L$ because of the necessity to have a fit number of impedance spectra. For the DMFA, instead the cost is given by:

$$\mathrm{Cost}_{DMFA} \propto L\cdot\log(L) + n_f \cdot n_Z \cdot \log(n_Z) \tag{10}$$

where L is the length of the dataset and n_f the number of multi-sine frequencies.

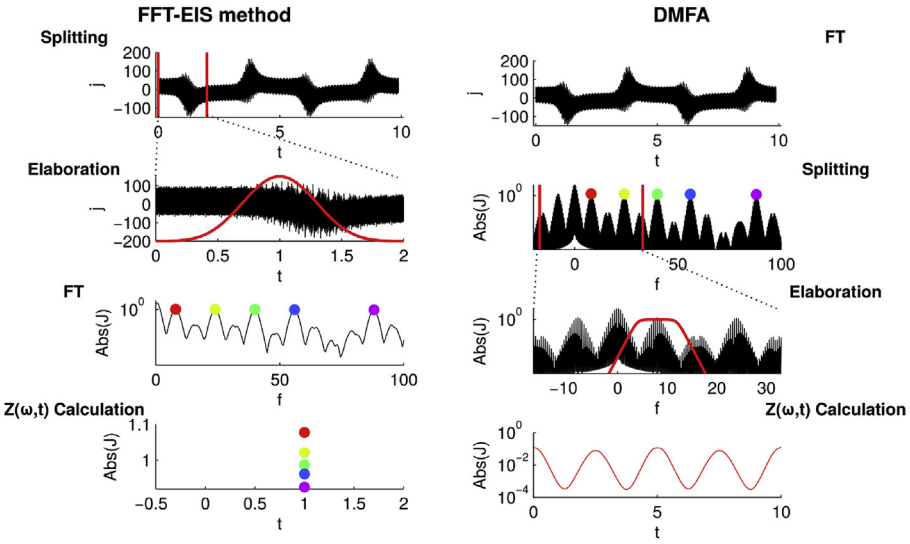

Fig. 1. Schematic comparison between FFT-EIS and DMFA.

As an example, the dataset used in this work has $L = 5$ MSample. We chose to extract 2000 spectra (n_Z), each one containing 35 frequencies (n_f). Due to the form of the broadband multi-sine signal, l_w is equal to 250,000 ($n_Z \cdot l_w = 5 \cdot 10^8$). Under these conditions, $\text{Cost}_{\text{FFT-EIS}}$ is almost hundred times larger than $\text{Cost}_{\text{DMFA}}$ (it still takes only a couple of seconds). The reason is in the low weight of many small FFT used in the *elaboration* step of the DMFA compared with many middle sizes FFT for the FFT-EIS method.

However, in the case of massive datasets, above 1 BSsamples, the costs of a single very large FFT and the memory requirements to handle such a calculation make FFT-EIS much more convenient.

2.4. Choice of the bandwidth

The choice of the bandwidth for the window function or the quadrature filter is important in order to recover the dynamic impedance with the highest possible precision. This influences also the choice of the frequencies in the multi-sine signal, especially the lowest one. We take as an example a simulated dataset made of a fast redox couple. On this redox couple two cycles of a quasi-cyclic voltammetry at 200 mV s^{-1} were performed. Details of the simulation can be found in the previous works [17]. Fig. 2 shows the potential and the current density of quasi-cyclic voltammetry in time (a and c) and in the frequency domain (b and c). The choice of the lowest frequency of the multi-sine signal should be tuned on the characteristic of the CV and in particular on its bandwidth. The necessary bandwidth can be measured from the Fourier transform of the input (potential) and of the output (current). It is the highest frequency around zero, which is necessary to capture "most of the signal". This is an arbitrary selection, and we have intended for "most of the signal" that at least 99.9% of the signal is included inside the bandwidth.

In our example in Fig. 2, the chosen bandwidth is 4 Hz, and this is what we will use also in the analysis of the data. As already observed in the precedent studies, the bandwidth is mainly determined by the shape of the potential [17]. The lowest frequency of the multi-sine signal is double the bandwidth [20], which for our example is 8 Hz. As explained, this value is strongly dependent on the type of system and *dc* signal and it should always be determined prior to the multi-sine experiment.

In this way it is possible to have a first estimation of the maximum resolution achievable. The *dc* and any other frequency of the multisine have similar skirt width. The skirt of the *dc* represents a background increase for the first multisine frequency and *vice versa*. Taking the first frequency at 8 Hz the skirts of the multisine frequency would be raised by circa 10^{-6} V in the potential and 10^{-4} A m^{-2} in the current density. However lowering the first frequency to 6 Hz would produce a raising of the background at 3 Hz of almost an order of magnitude both in the potential and in the current.

Based on this discussion a multisine covering 5 decades (8 Hz–100 kHz) with 35 frequencies with a minimum distance of 8 Hz was taken (see also reference [20]).

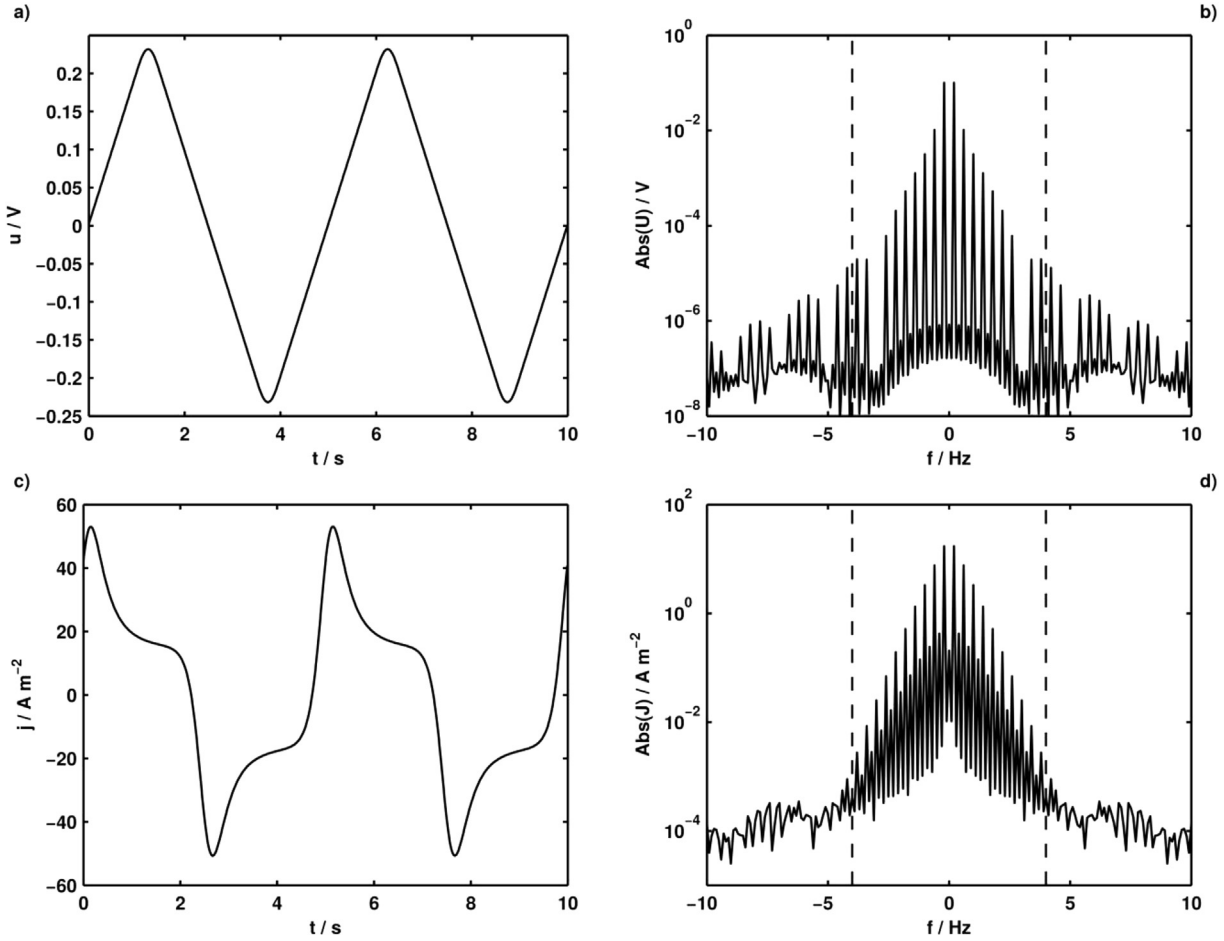

Fig. 2. Quasi-cyclic voltammetry. Potential (a) and current density (c) in the time domain. Potential (b) and current density (d) with bandwidth limit of 4 Hz in the F-domain.

2.5. How to recover Z(ω,t)

In this section we will discuss the shape of the window function and of the quadrature filter. The window function used in the FFT-EIS is typically the Blackmann-Harris periodic window [26]:

$$w\left(t^{'}-t,bw\right)=a_0+a_1\cdot\cos\left[2\cdot\pi\cdot bw\cdot\left(t^{'}-t\right)\right]+a_2\cdot\cos\left[4\cdot\pi\cdot bw\cdot\left(t^{'}-t\right)\right]+a_3\cdot\cos\left[6\cdot\pi\cdot bw\cdot\left(t^{'}-t\right)\right] \quad (11)$$

where the a_i's values are equal to: $a_0=0.35875$; $a_1=0.48829$; $a_2=0.14128$; $a_3=0.01168$ (taken from Matlab® version 2013a). We will use this one in the manuscript for comparing the strategies for the extraction of dynamic impedance spectra.

The quadrature filter has a rectangular or quasi-rectangular shape with rounded borders. We obtained the given form by multiplying two Fermi-Dirac functions and normalizing the value at the central frequency to one. The final result is mathematically given by the expression:

$$\tilde{g}\left(\omega^{'}-\omega,bw\right)=\frac{[1+\exp(-n)]^2}{\left[1+\exp\left(-n\cdot\frac{\omega^{'}-\omega+bw}{bw}\right)\right]\cdot\left[1+\exp\left(n\cdot\frac{\omega^{'}-\omega-bw}{bw}\right)\right]} \quad (12)$$

where n is a factor determining the shape of the filter and it was taken equal to eight. In Fig. 3 the form of the window function and the quadrature filter is shown in the frequency and in the time domain. In the case of the window function, we show different values of the *bw*, which correspond also to different amount of integration periods. It is clear that in order to reach a bandwidth of maximum 4 Hz, the integration time has to be at least 2 periods.

3. Results

The comparison between the FFT-EIS method and the DMFA is performed on the same simulated dataset but in two different ways. The multisine is the same in both cases. In the first case a perfectly periodic dataset is selected. This comprises two periods of the quasi-cyclic voltammetry. In the second case, the dataset is not periodic and covers only 1.5 periods. In both cases the results of the FFT-EIS and DMFA are also compared with the ideal calculation of the dynamic impedance given by the set of Eqs. (5) and (6). For the FFT-EIS the results are given following the method of Bond which simply employs a window function and also following the method of Harrington, which takes also advantage of a baseline correction.

Fig. 4 shows the results of the recovered cyclic voltammetry for the periodic case. In the case of the DMFA with a quasi-rectangular filter of bandwidth 4 Hz the difference between the recovered curve and the ideal case, without multisine, is below 0.2%.

The results of Bond and Harrington are the same since there is no baseline correction on the *dc* component. For a 2-periods window function (FFT-EIS 2 p.) the CV is noisy but close to the ideal case as the −3 dB bandwidth is circa 4 Hz, but it rolls off too slowly (see

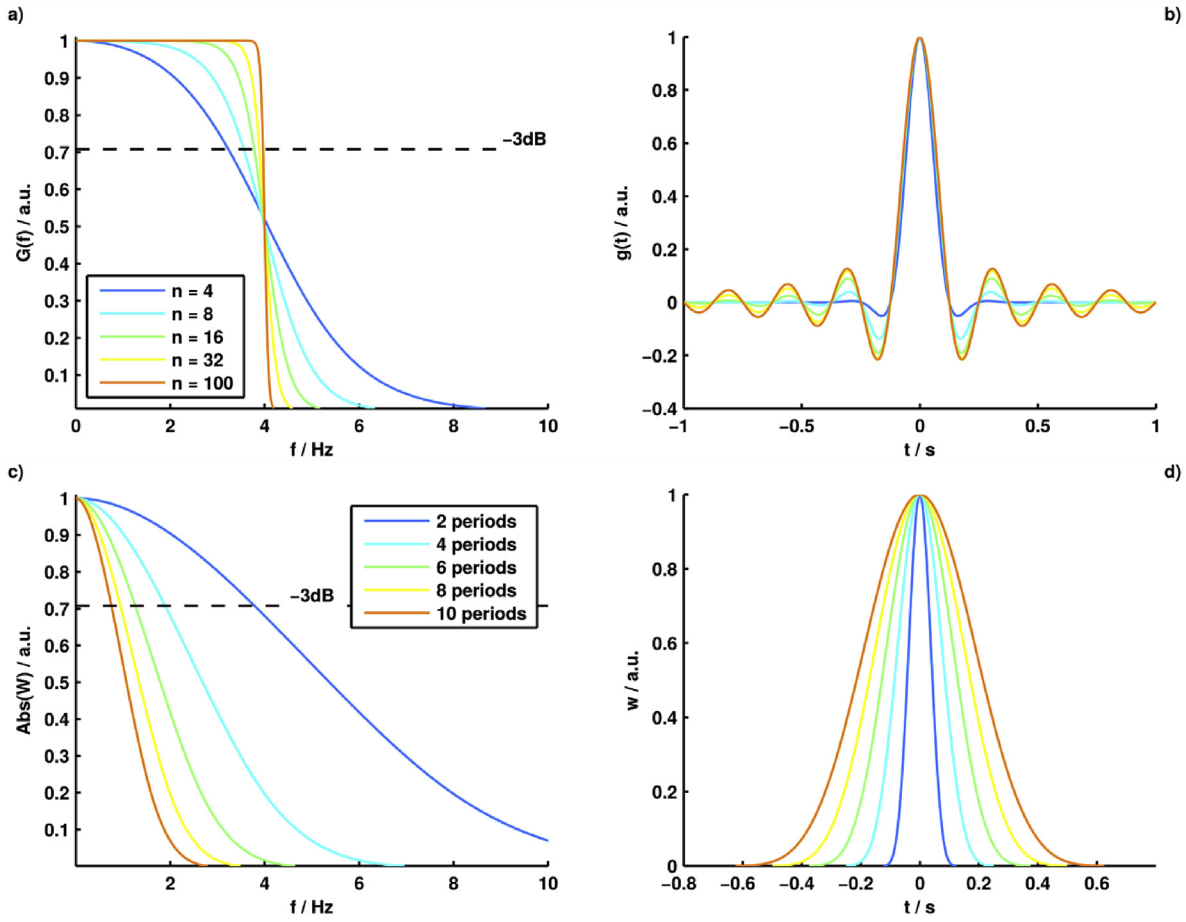

Fig. 3. Frequency and time representation of the filter and of the window function. Rectangular filter in the frequency domain (a) and in the time domain (b) at a fixed bandwidth of 4 Hz and different values of the parameter *n*. Window function in the frequency domain (c) and in the time domain (d) as function of its temporal width. All curves are normalized to unitary magnitude.

Fig. 3c) which inevitably takes in some interferences from the first multisine frequency. The 4-periods window (FFT-EIS 4 p.), with a −3 dB bandwidth of circa 2 Hz (see Fig. 3c), is a low-passed filtered version of the previous one, which is also smoother.

The results of the dynamic impedance are reported in Fig. 5. In particular, a detail of the first frequency (8 Hz) is shown in Fig. 5a. The trend for the methods proposed by Bond and Harrington (4-periods width) and the DMFA (4 Hz bandwidth) are the same. However there are some discrepancies between the FFT-EIS methods and the ideal dynamic impedance, while even at this magnification the DMFA and the ideal dynamic impedance are barely distinguishable. Fig. 5b illustrates the average relative difference between the ideal dynamic impedance and those calculated with the various methods. For the DMFA the difference is circa 1% for the first frequency and goes below 0.1% for the last frequencies. In the FFT-EIS case both for Bond and for Harrington the first frequency cannot be recovered with a window width of 2 periods, but in general these results are much better than those recovered with a 4-periods window. The reason is given by the low pass filtering effect of the wider window.

In all cases the relative error decreases rapidly for higher frequencies, a phenomenon in line with what already observed, *i.e.* it is easier to recovery the dynamic impedance at frequencies far from the *dc*.

3.1. Non-periodic case

The non-periodic dataset consists of 1.5 periods of the quasi cyclic voltammetry. In this case the skirt of the *dc* component increases due to Gibbs phenomenon and strongly overlaps with the signal of the multi-sine. Fig. 6 shows this phenomenon which can be ameliorated mirroring the dataset around its last point, thus doubling the length of the dataset. Similar methods are used in digital image elaboration.

Fig. 6a and b shows the frequency domain of the voltammetry without multisine. Both in part (a), which shows the potential, and in part (b), which shows the current density, the skirt of the voltammetry is orders of magnitude higher than in Fig. 2a and b. At the selected bandwidth of 4 Hz the intensity of the potential and of the current decreased of only three and two orders of magnitude respectively against the six and four of Fig. 2.

The Fourier transform of a mirrored dataset presents some particular features. First, it contains double the amount of points, as

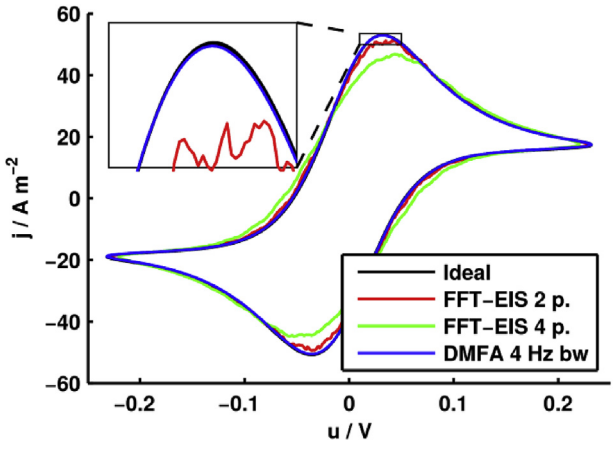

Fig. 4. Cyclic voltammetry recovered with windowing (FFT-EIS) and filtering (DMFA) compared with the ideal data.

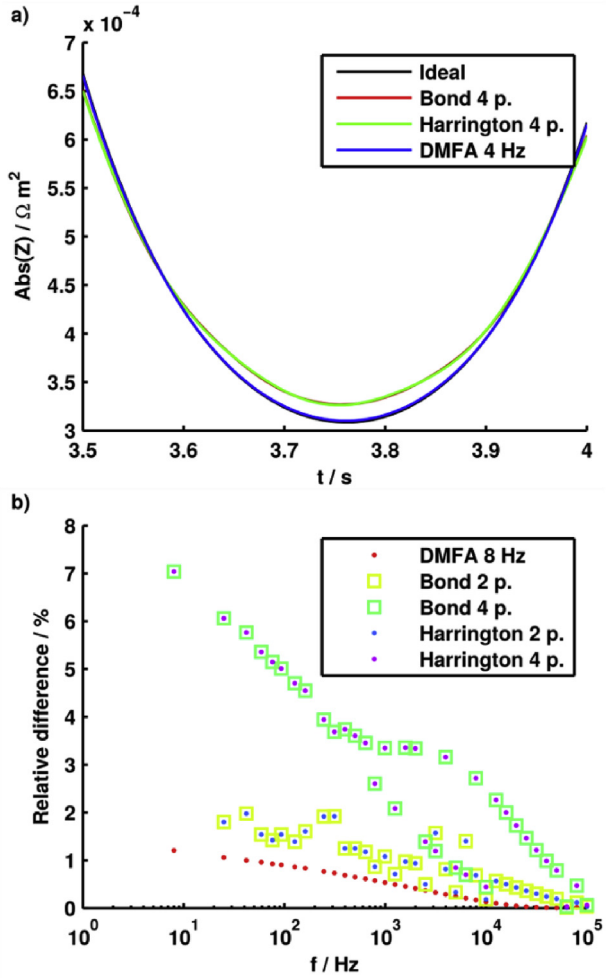

Fig. 5. a) particular of dynamic impedance for the first frequency (8 Hz) recovered with windowing (4-periods width) and filtering (4 Hz bandwidth) compared with the ideal data. b) average relative difference between the different methods and the ideal impedance as function of the multisine frequency (note: Bond and Harrington overlap).

the dataset is twice as long now, and half of these points fall at frequencies in between those of the original dataset. This is particular evident in Fig. 6a, where half points almost perfectly overlaps with those of the original non-periodic dataset and the other half falls at lower amplitude (circa 10^{-8}, not visible), especially away from the zero frequency.

On the current (Fig. 6b), the effect of the mirroring on the voltammetry skirt is remarkable. In fact at the selected bandwidth the skirt intensity dropped of an order of magnitude. While initially with a 4-Hz bandwidth more than 99.9% of the voltammetry intensity fell inside the bandwidth limits, with a non-periodic dataset this value dropped to 98.7% for the potential and 63.3% for the current density. This means that a larger part of the *dc* skirt affects the first multisine frequencies. However, after mirroring these percentage went to 98.8 and 97.0%.

The difference is more evident in the current because the discrepancy between the first and last point in the potential in the particular case of 1.5 periods is small, while it is much larger in the current.

The non-periodicity and in general discontinuities between the beginning and the end of the dataset is not a problem for the FFT-

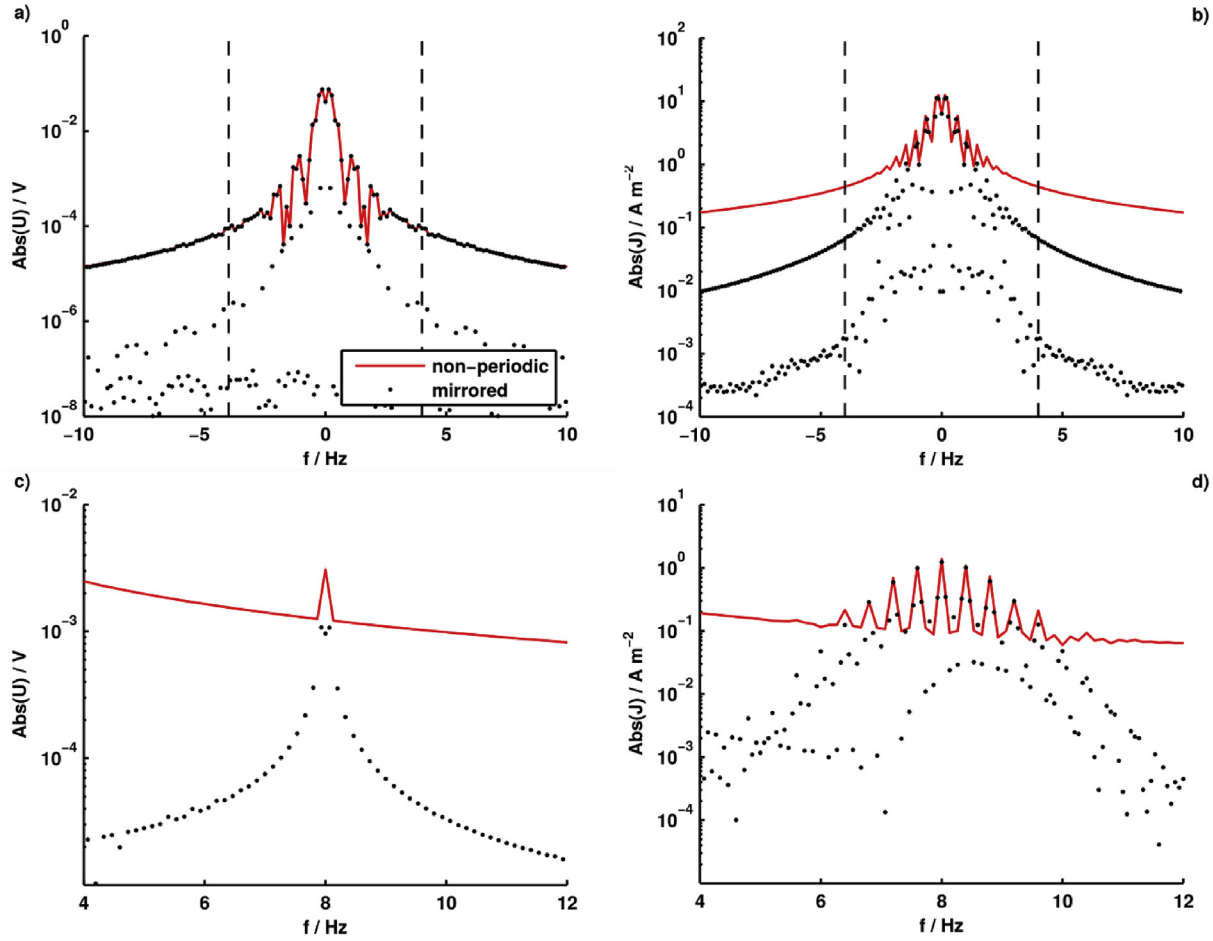

Fig. 6. Frequency representation of the non-periodic dataset with and without mirroring. Quasi cyclic voltammetry without multisine: potential (a) and current density (b). Comparison between the non-periodic (1.5 p. CV) and the mirrored datasets (mirrored 1.5 p. CV) in correspondence of the first multisine frequency: potential (c) and current density (d).

EIS methods since the dynamic impedance is calculated independently on single sections of the dataset. However, in the case of the DMFA, the increase of the *dc* skirt can completely submerge the first multisine frequencies as shown in Fig. 6c and d. In particular, in the case of the potential, the 8 Hz peak is only a factor of two higher than the background (Fig. 6c), while in the current density its intensity is only an order of magnitude above the background (Fig. 6d). Nevertheless after mirroring clear peaks appear in both cases.

The results of the dynamic impedance for three frequencies are displayed in Fig. 7 which shows the first, the fifth, and the eleventh frequency of the multisine. Without mirroring a part of the dataset corresponding to circa twice the bandwidth (0.5 s) is lost because of the distortions introduced by the raising of the *dc* skirt. However after mirroring the artifacts are reduced and only a part of the dataset in the time domain equal to $1/bw$ is lost. Because the distortions derive from the broadening of the *dc* skirt the higher the frequencies of the multisine the less affected they are.

It is noteworthy that although the FFT-EIS methods are not affected by the non-periodicity of the dataset and no particular ploy is necessary, a part of data is anyway lost. In fact half window width is lost at the beginning and at the end of the dataset because the dynamic impedance is calculated as the middle point of the window. In the case of the 2-periods (referred to the lowest multisine frequency) width, this loss is 0.25 s per side.

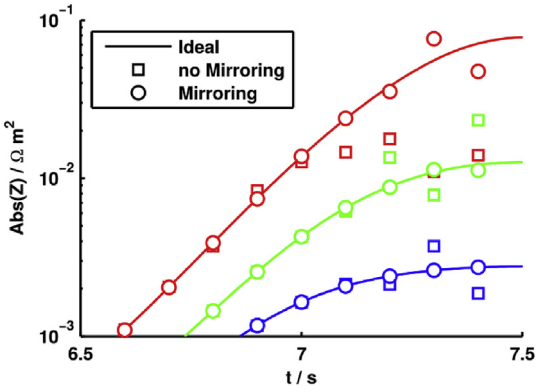

Fig. 7. Effect of mirroring on a non-periodic dataset. Frequencies: 8 Hz (red), 76 Hz (green), and 399 Hz (blue). (For interpretation of the references to colour in this figure legend, the reader is referred to the web version of this article.)

4. Summary and conclusions

In this manuscript we derived the dynamic admittance $Y(\omega,t)$ as the first order approximation of a Volterra series associated to a time-variant potential perturbation. With this definition it was possible to calculate directly the dynamic impedance from the

constituent equations of the system as an ideal case unaffected by any methodological limitation. This ideal dynamic impedance represents the limit toward which the heuristic definition tends. Based on this, a comparison among different methods used to recover the dynamic impedance was made.

Based on literature, two main methodologies exist to recover the dynamic impedance. The first one named FFT-EIS is based on the use of window functions. The second one, named dynamic multi-frequency analysis (DMFA), instead employs quadrature filters.

It was shown that the FFT-EIS method suffers of the poor bandwidth of the window function in respect to its temporal length, especially at the lowest frequencies. Contrary, the DMFA offers the advantage of employing all the dataset at once which also allows digital filters with sharp bandwidth. At higher frequencies the difference between the FFT-EIS and the DMFA decrease and in this particular case above 1 kHz the respective difference with the ideally-calculated dynamic impedance was below 1.5 and 1%, respectively.

On the other hand, if the dataset is not periodic, several distortions are introduced at the beginning and at the end of the dynamic impedance calculated by the DMFA, while the FFT-EIS is not affected by the general shape of the dataset. To overcome this limitation a mirroring of the dataset is necessary before performing the DMFA, which greatly reduces but not eliminates the distortions and their length.

The two different strategies appear to be both well suited for recovering the dynamic impedance spectra, with DMFA showing a slightly better capability to deal with lower frequencies.

Acknowledgement

This project has received funding from the European Research Council (ERC) under the European Union's Horizon 2020 research and innovation programme (grant agreement n° 772579).

Appendix A. Supplementary data

Supplementary data related to this article can be found at https://doi.org/10.1016/j.electacta.2019.03.033.

References

[1] S.C. Creason, D.E. Smith, Fourier transform faradaic admittance measurements: I. Demonstration of the applicability of random and pseudo-random noise as applied potential signals, J. Electroanal. Chem. Interfacial Electrochem. 36 (1972) A1–A7, https://doi.org/10.1016/S0022-0728(72)80466-2.

[2] S.C. Creason, J.W. Hayes, D.E. Smith, Fourier transform faradaic admittance measurements III. Comparison of measurement efficiency for various test signal waveforms, J. Electroanal. Chem. Interfacial Electrochem. 47 (1973) 9–46, https://doi.org/10.1016/S0022-0728(73)80343-2.

[3] S.C. Creason, D.E. Smith, Fourier transform faradaic admittance measurements II. Ultra-rapid, high precision acquisition of the frequency response profile, J. Electroanal. Chem. Interfacial Electrochem. 40 (1972) A1–A5, https://doi.org/10.1016/S0022-0728(72)80146-3.

[4] A.M. Bond, R.J. Schwall, D.E. Smith, On-line FFT faradaic admittance measurements application to A.C. cyclic voltammetry, J. Electroanal. Chem. Interfacial Electrochem. 85 (1977) 231–247, https://doi.org/10.1016/S0022-0728(77)80290-8.

[5] J. Házì, D.M. Elton, W.A. Czerwinski, J. Schiewe, V.A. Vicente-Beckett, A.M. Bond, Microcomputer-based instrumentation for multi-frequency Fourier transform alternating current (admittance and impedance) voltammetry, J. Electroanal. Chem. 437 (1997) 1–15, https://doi.org/10.1016/S0022-0728(96)05038-3.

[6] G.S. Popkirov, R.N. Schindler, Optimization of the perturbation signal for electrochemical impedance spectroscopy in the time domain, Rev. Sci. Instrum. 64 (1993) 3111–3115, https://doi.org/10.1063/1.1144316.

[7] K. Darowicki, J. Orlikowski, G. Lentka, Instantaneous impedance spectra of a non-stationary model electrical system, J. Electroanal. Chem. 486 (2000) 106–110, https://doi.org/10.1016/S0022-0728(00)00111-X.

[8] K. Darowicki, J. Orlikowski, A. Arutunow, Investigations of the passive layer cracking by means of dynamic electrochemical impedance spectroscopy, Electrochim. Acta 48 (2003) 4189–4196, https://doi.org/10.1016/S0013-4686(03)00604-2.

[9] K. Darowicki, P. Ślepski, Dynamic electrochemical impedance spectroscopy of the first order electrode reaction, J. Electroanal. Chem. 547 (2003) 1–8, https://doi.org/10.1016/S0022-0728(03)00154-2.

[10] K. Darowicki, P. Ślepski, M. Szociński, Application of the dynamic EIS to investigation of transport within organic coatings, Prog. Org. Coating 52 (2005) 306–310, https://doi.org/10.1016/j.porgcoat.2004.06.007.

[11] R.L. Sacci, D. Harrington, Dynamic electrochemical impedance spectroscopy, ECS Trans. 19 (2009) 31–42, https://doi.org/10.1149/1.3247564.

[12] R.L. Sacci, D. Harrington, Dynamic impedance of formic acid electrooxidation on polycrystalline palladium, ECS Trans. 19 (2009) 123–129, https://doi.org/10.1149/1.3247570.

[13] D.A. Harrington, Dynamic and coverage effects in EIS (Invited), ECS Trans. 45 (2013) 3–14, https://doi.org/10.1149/04513.0003ecst.

[14] R.L. Sacci, F. Seland, D.A. Harrington, Dynamic electrochemical impedance spectroscopy, for electrocatalytic reactions, Electrochim. Acta 131 (2014) 13–19, https://doi.org/10.1016/j.electacta.2014.02.120.

[15] T. Holm, P.K. Dahlstrøm, S. Sunde, F. Seland, D.A. Harrington, Dynamic electrochemical impedance study of methanol oxidation at Pt at elevated temperatures, Electrochim. Acta 295 (2019) 139–147, https://doi.org/10.1016/j.electacta.2018.10.071.

[16] K. Darowicki, Theoretical description of the measuring method of instantaneous impedance spectra, J. Electroanal. Chem. 486 (2000) 101–105, https://doi.org/10.1016/S0022-0728(00)00110-8.

[17] D. Koster, G. Du, A. Battistel, F. La Mantia, Dynamic impedance spectroscopy using dynamic multi-frequency analysis: a theoretical and experimental investigation, Electrochim. Acta 246 (2017) 553–563, https://doi.org/10.1016/j.electacta.2017.06.060.

[18] R.G. Lyons, Understanding Digital Signal Processing, third ed., Prentice Hall, 2010. http://proquest.safaribooksonline.com/9780137028450. (Accessed 27 April 2017).

[19] S. Boyd, L.O. Chua, C.A. Desoer, Analytical foundations of Volterra series, IMA J. Math. Control Inf. 1 (1984) 243–282, https://doi.org/10.1093/imamci/1.3.243.

[20] A. Battistel, G. Du, F. La Mantia, On the analysis of non-stationary impedance spectra, Electroanalysis 28 (2016) 2346–2353, https://doi.org/10.1002/elan.201600260.

[21] M.E. Orazem, B. Tribollet, Electrochemical Impedance Spectroscopy, Wiley, Hoboken; N.J, 2008. http://www.worldcat.org/oclc/144517368.

[22] A. Battistel, F. La Mantia, Nonlinear analysis: the intermodulated differential immittance spectroscopy, Anal. Chem. 85 (2013) 6799–6805, https://doi.org/10.1021/ac400907q.

[23] A. Battistel, F. La Mantia, Intermodulated non-linear analysis of a redox couple in solution. 1. The model, Electrochim. Acta 176 (2015) 1484–1491, https://doi.org/10.1016/j.electacta.2015.07.138.

[24] A. Battistel, A. Petkovic, F. La Mantia, Intermodulated non-linear analysis of a redox couple in solution. 2. Experimental results, Electrochim. Acta 176 (2015) 1492–1499, https://doi.org/10.1016/j.electacta.2015.07.139.

[25] T. Breugelmans, J. Lataire, T. Muselle, E. Tourwé, R. Pintelon, A. Hubin, Odd random phase multisine electrochemical impedance spectroscopy to quantify a non-stationary behaviour: theory and validation by calculating an instantaneous impedance value, Electrochim. Acta 76 (2012) 375–382, https://doi.org/10.1016/j.electacta.2012.05.051.

[26] F.J. Harris, On the use of windows for harmonic analysis with the discrete Fourier transform, Proc. IEEE 66 (1978) 51–83, https://doi.org/10.1109/PROC.1978.10837.